



Grant agreement no. 312818  
SPA.2012.2.2-01 : Key technologies enabling observations in and from space

- Collaborative project -

WP 3 – Interferometer Instrument Technology Development

## D3.4 Note on Alternative Interferometer Techniques

Due date of deliverable: month 25

Actual submission date:

Start date of project: January 1<sup>st</sup> 2013

Duration: 36 months

Lead beneficiary for this deliverable: UCL

Last editor: N.Baccichet, University College London (UCL)

Contributors:

N.Baccichet (UCL), G. Savini (UCL).

Project co-funded by the European Commission within the Seventh Framework		
<b>Dissemination Level</b> (please refer to the list of deliverables in Annex 1 and complete		
PU	Public	
PP	Restricted to other programme participants (including the Commission	
RE	Restricted to a group specified by the consortium (including the	
CO	Confidential, only for members of the consortium (including the Commission Services)	

## History table

Version	Date	Released by	Comments
1	19 <sup>th</sup> January	UCL	First issue – section 4 is incomplete awaiting input from NB. References partially complete. Section 5 is TBW pending completion section 4.
2 (Final)	30 <sup>th</sup> March	UCL	Final Issue

## Table of contents

1	Introduction.....	5
1.1	Scope .....	5
1.2	Introduction.....	5
2	Sparse Aperture Systems.....	5
2.1	Radio Heterodyne Interferometers.....	7
3	Mathematics of Direct Detection Interferometers .....	8
3.1	Focal plane recombination:.....	8
3.2	Pupil Plane Recombination:.....	10
3.3	The u-v Plane and the Visibility Function .....	11
3.4	The “Double-Fourier” method .....	11
3.5	The FISICA Study Selection .....	12
4	Focal plane recombination in more detail .....	13
4.1	Golay non-redundant arrays.....	13
4.1.1	Optical theory .....	14
4.2	Feasibility studies and Implementations.....	17
4.3	Error analysis for Golay arrays.....	18
4.3.1	Piston Error .....	19
4.3.2	Tilt Error .....	21
4.3.3	Pupil Mapping Error.....	23
4.3.4	Comparison between a Golay-6 system and FIRI.....	25
4.4	Pupil densification .....	27
4.5	Minimum redundancy linear arrays .....	30
5	Summary – pursuing technical implementation of Michelson .....	31
6	Bibliography.....	33

## **Acknowledgements**

The research leading to this report has received funding from the European Union 7th Framework Programme SPA.2012.2.2-01 under grant agreement number 312818.

## **Disclaimer**

The content of this deliverable does not reflect the official opinion of the European Union. Responsibility for the information and views expressed in the deliverable therein lies entirely with the author(s).

# 1 Introduction

## 1.1 Scope

This document reviews the methods available for the direct combination of light from sparsely separated apertures to allow increased spatial resolution for astronomical observations in the Far Infrared wavelength band. The emphasis is on non-phase sensitive detection i.e. we only briefly touch on heterodyne detection methods.

## 1.2 Introduction

The spatial resolution of any optical imaging system used for astronomy is determined by the widest separation of any collecting area used to concentrate the light compared to the wavelength of the light being measured. Thus the spatial resolution of a traditional solid telescope is limited by the physical diameter of the system to  $\sim\lambda/D$ ; where  $\lambda$  is the wavelength and  $D$  the telescope diameter. The limitations imposed by solid telescopes can be overcome by using sparsely separated elements and recombining the light to make a “synthetic” aperture that appears to have a much larger diameter than any of the individual elements. This technique is generally known as spatial interferometry.

# 2 Sparse Aperture Systems

A useful methodology for characterising different types of recombination of signals from sparsely distributed apertures is offered by van der Avoort et al (2007 [1]). We illustrate the four different basic methods in Figure 1.

These can be described as follows:

- a) Focal plane recombination (Fizeau) interferometer where the pupil plane is kept “right sized” such that the light is combined in phase as if it had come from small apertures placed over a single aperture. In fact this is the exact method employed by Michelson in measuring the measuring the first stellar diameters using the Mount Palomar 100 inch telescope. As this is termed the

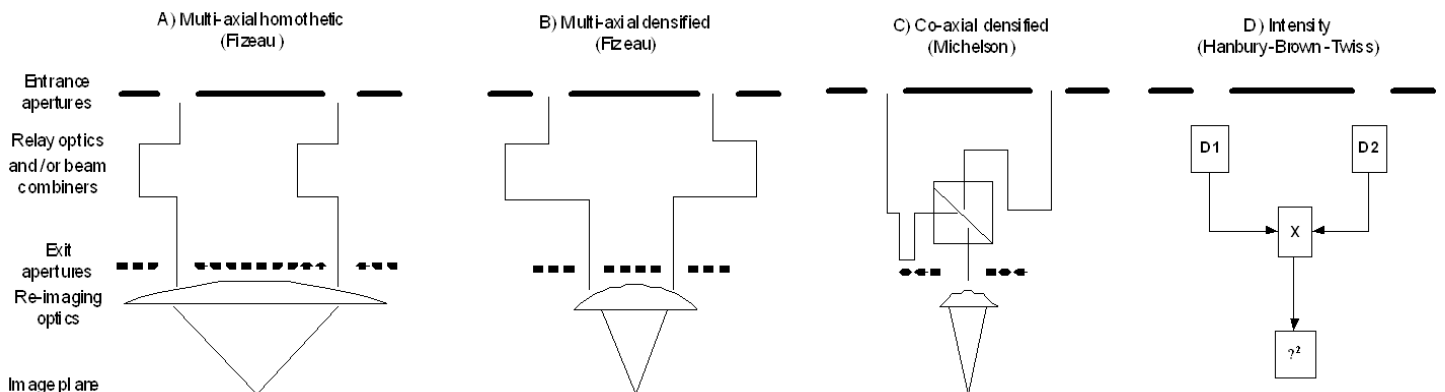


Figure 1: Diagrams illustrating four basic method of recombining the signals from sparsely distributed apertures to synthesise a single large one.

## Far Infra-red Space Interferometer Critical Assessment

- “Michelson stellar interferometer” in much of the literature (and is the technique used for instance in the VLT) we will call both this, and the densified pupil version, “Focal Plane Recombination” interferometers.
- b) “Homothetic” systems have the limitation that the sparse apertures have to be kept a long way apart thus making the system unwieldy in many circumstances (especially for space deployment and at long wavelengths). The densified pupil arrangement for focal plane recombination interferometers has therefore been proposed (see Labeyrie, Lipson, and Nisenson [2] ) whereby the image of the apertures is rearranged in a secondary pupil plane still keeping the signals from the different apertures in phase. In this way it is supposed that the resolution of the synthesised sparsely distributed apertures is maintained whilst concentrating the recombination optics in a more convenient form. We discuss this arrangement further in section 4 as it potentially offers an alternative solution to pupil plane recombination.
  - c) The pupil plane direct detection interferometer technique uses the true Michelson interferometer although for reasons given above we will call this the “Pupil Plane Interferometer”. Here the signals from two (classically defined) apertures are brought together in phase at an overlapping image of the sparsely distributed apertures and, by a combination of aperture movement and phase difference tracking with a moving mirror system, the “fringe visibility” of the source is recovered. Little more needs to be said about this system as it is the subject of extensive investigation – in a “double Fourier” guise – as part of the FISICA programme. As an aside the “double Fourier” refers to the use of a second moving mirror system that is used to simultaneously measure the spectral content of the light in addition to the phase tracking for spatial reconstruction.
  - d) The last method that is worthy of brief consideration in this context is the intensity interferometer. Here the method does not rely on keeping the light from the apertures in phase but rather on using the quantum correlation of the photons seen within the coherence time of the light emitted from the source (see Hanbury-Brown and Twiss, 1958 [3]). This coherence time can also be thought of as the “photon occupation number” in correlation spectroscopy as discussed by Zmuidzinas, (2003 [4]) *App Opt*, 42 (2003). Hanbury-Brown and Twiss successfully used an intensity interferometer [5] to measure the diameters of a number of stars however, the difficulties in using the technique at optical wavelengths soon became apparent (essentially the occupation number is far too small for any reasonably sized system to have a sensible sensitivity) and the technique was abandoned in favour of Michelson interferometers. However, at longer wavelengths and for certain source types the occupation number rapidly increases and with very fast detection systems it would be possible to use an intensity interferometer (see for instance [2], [6], [7]). In the radio intensity interferometers would also work very well but are essentially redundant with the use of direct signal detection using fast amplifiers. For our purposes – i.e. in considering FIR applications – we can ignore the technique as the detection systems available are nowhere near fast enough (multiple GHz response times are required) for any correlation to be detectable.

After this brief introduction on types of direct detection techniques we will go on to discuss the mathematics behind interferometry in more detail in section 3. We will take a more detailed look at sparse aperture focal plane recombination in section 4 and provide some concluding remarks in section 5. First, whilst it is not the subject of the FISICA study being the most popular of radio interferometer techniques, we give an overview of the alternative heterodyne interferometer tech in the next sub-section.

## 2.1 Radio Heterodyne Interferometers

Interferometry has been successfully employed since the 1950's at radio wavelengths to make very large effective diameter telescopes with extremely high spatial resolution. Over many decades the wavelengths at which these systems operate have gradually decreased to the extent that the ALMA facility now operates routinely at  $\sim 450 \mu\text{m}$ , and in principle it could operate at  $200 \mu\text{m}$  with an enhanced receiver capability. The limitations on operating at shorter wavelengths are imposed by the transmission of the atmosphere rather than any fundamental technical issues. The receivers used in radio interferometers either use direct amplification of the signals (at long wavelengths i.e. low frequencies) or what is known as heterodyne reception whereby the incoming signal is compared – “mixed” – with a local reference (termed the local oscillator) to produce an intermediate frequency signal that can be analysed using standard electronics. Although there are possibilities of building heterodyne, and even direct amplifier, receivers at the wavelengths of interest in the FIR there are a number of issues that must be considered:

- The most basic feature of heterodyne systems is that they are inherently spectrally narrow banded ( $R \gg 10^6$ ) and are therefore not suitable for many of the science cases identified in [8]. They are however excellent for the study of astrophysical chemistry and, with sufficient numbers of dishes, have been used to make images of dust emission [9].
- The ultimate sensitivity of heterodyne systems is limited by quantum fluctuations due to their high spectral resolution and use of lasers as local oscillators. This is especially true at optical and infrared wavelengths (the “quantum limit” – e.g. [10] as discussed further below).
- Direct amplification of incoming signals in the THz is not yet routinely available for any applications. Although there has been progress in developing parametric amplifiers working at high frequencies, these are in their infancy and cannot be considered for studying an interferometer at the present time as too little is known about their possible performance characteristics (e.g. [11]. See also the discussion on intensity interferometers above).
- Finally, there are a number of difficult technical problems with implementing a heterodyne interferometer in space that are at least as challenging as those associated with a direct detection system. These deserve and need a full study much like FISICA – see for instance the ESPRIT study [12].

For these reasons, especially the last, we have not conducted a detailed comparison between a direct detection and heterodyne space interferometer within the ambit of

## Far Infra-red Space Interferometer Critical Assessment

FISICA. Rather we discuss here, briefly, the limitations of the sensitivity of a heterodyne system operating in the FIR. The quantum limit is given in units of brightness temperature by  $h\nu/k_b$ . We take as our reference wavelength the OI[63um] line which is equivalent to 4.7 THz giving  $T_{lim} \sim 225$  K. If we assume that a full-fledged space interferometer will have four 3 m dishes [12], and that the correlation is linear such that the sensitivity scales as  $\sqrt{N_{dishes}}$ : then this equates to a line sensitivity of  $\sim 1 \times 10^{-20}$  W m<sup>-2</sup> for a one hour observation. Compare this to a direct detection system limited only by the natural Zodiacal background (e.g. [13]) which even with a single 3.5 m dish will reach the same detection limit. We can see then that, assuming all technical issues can be addressed in either system, to first order a heterodyne system will have to have much greater total area driving the possible cost and complexity. In reality the detailed science case for direct detection versus a heterodyne system is rather different. For instance, it is only with the very high spectral resolution offered by heterodyne detection that one can probe the detailed molecular chemistry and conduct studies into velocity structures associated with star and planetary formation. On the other hand the detection of dust, solid state features and tracing the various phases of the ISM in extragalactic sources is better suited to a direct detection system [8].

As stated in the goals of the FISICA project we concentrate here on the science and technical case for a direct detection interferometer and for the remainder of this document we discuss possible different implementations.

### 3 Mathematics of Direct Detection Interferometers

---

Here we briefly review the key mathematical equations that govern the response of focal plane and pupil plane interferometers in order to illustrate the key differences behind the concepts. This of necessity a very brief overview and the reader is referred to more extensive reviews ( [2], [14])

#### 3.1 Focal plane recombination:

The basic operation of a focal plane recombination system is identical to Young's slit experiment as shown by Born and Wolf [15] in describing what they term the "diffractometer". Figure 2 shows a simplified diagram of the diffractometer which shows immediately the analogy with Young's slits.

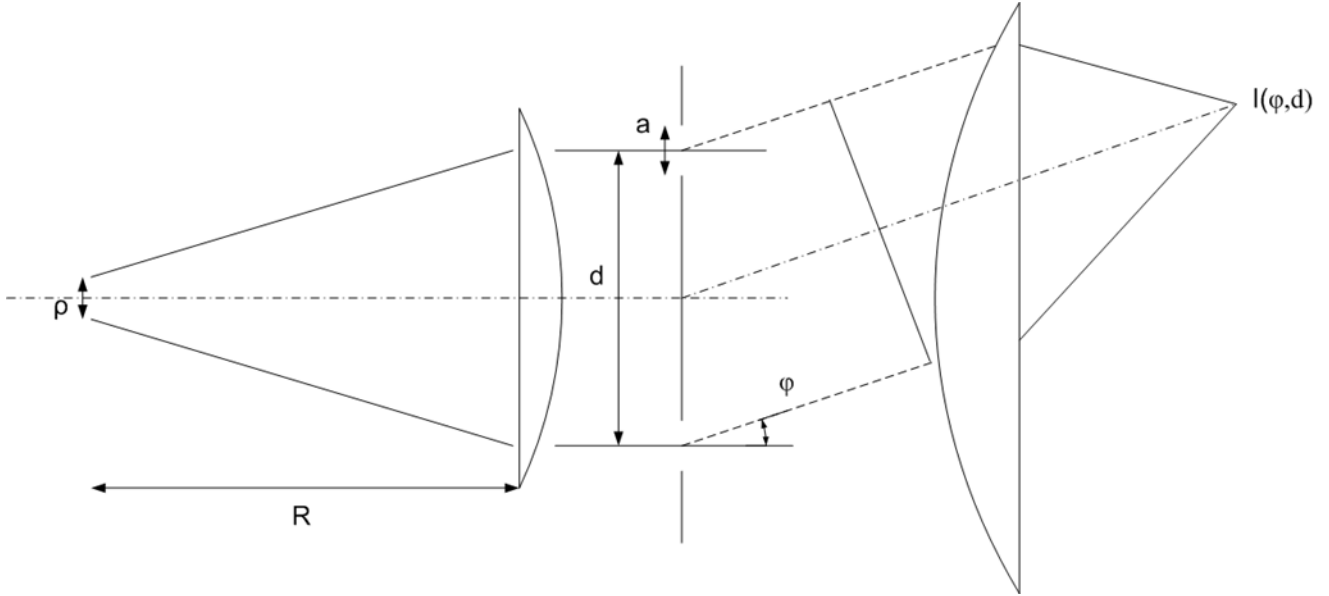


Figure 2: The basic layout of the Born and Wolf diffractometer. In practice in an astronomical observation,  $R$  is infinite and only the angle subtended by the source is of interest.

The intensity observed at the image plane is given by:

$$I(\phi, d) = 2 \left( \frac{2J_1(u)}{u} \right)^2 \left\{ 1 + \frac{2J_1(v)}{v} \cos \left( \beta(v) - \frac{2\pi}{\lambda} d \sin \phi \right) \right\} \quad (1)$$

Where,

$$u = \frac{2\pi}{\lambda} a \sin \phi, \quad v = \frac{2\pi \rho d}{\lambda R} \quad \text{or}$$

$$v = \frac{\pi d \theta}{\lambda}$$

if  $R$  is essentially infinite and  $\theta$  is the subtended source size.

$$\beta(v) = 0 \quad \text{when} \quad \frac{2J_1(v)}{v} > 0 \quad \text{or} \quad \pi \quad \text{when} \quad \frac{2J_1(v)}{v} < 0$$

The two important terms here are  $\frac{2J_1(v)}{v}$  which represents the mutual coherence function  $\gamma_{12}$  of the source (here a Bessel function as the source is assumed circular) and  $\left( \frac{2J_1(u)}{u} \right)^2$  which is the “enveloping function” for the fringe visibilities and represents a measure of the field of view of the instrument. Note the latter is basically determined by the size of the individual apertures and is of order  $\sim \lambda/a$ . We discuss this further considering various real world effects and in the case of multiple apertures in section 4. The real part of the mutual coherence function,  $|\gamma_{12}|$ , represents, by the van Cittert-Zernike theorem [15], the Fourier transform of the spatial content of the source. We can see then that by measuring  $|\gamma_{12}|$  with different aperture spacings we can determine the source distribution at a number of spatial frequencies thus effectively reconstructing a direct image of the source. As we show later this can be done simultaneously by employing an array of apertures efficiently spaced across the

required pupil plane and reimaging the pupil plane onto a more convenient scale before finally recombining onto the image plane. Traub (1986 [16]) points out that, in order to maintain the full spatial sampling of any distributed array, the final pupil plane viewed from the image plane must appear to have come from a single masked aperture of the same size. He states this as the “golden rule” of aperture recombination and this restricts the ability to re-order the re-imaged pupil plane or “densify” it, apart from a linear change in the system magnification. We discuss the implications of this on schemes which employ densified pupils in section 4.

### 3.2 Pupil Plane Recombination:

The basic elements of a pupil plane recombination interferometer are shown in Figure 3. Here we show a ground based system where the telescope apertures are required to point towards the object from a fixed vertical baseline and therefore an optical delay line is required to remove the delay in arrival of the light from a source not at the zenith. In principle this would not be required from a space-based, structurally connected system where the baseline can be rotated to ensure the source of interested is always effectively at the zenith. The in-phase beams are then recombined using a simple beam splitter arrangement with or without a second adjustment for the phase control<sup>1</sup>. The combined signals are then sent to a detector. In a classical arrangement the distance  $d$  is varied and the optical delay line is used to track the interference fringe.

In practice in ground based interferometers (VLTI for instance), a number of primary dishes are used in a semi-stationary arrangement thus only partially replicating a filled aperture. In all ground based systems the rotation of the Earth is used to fill as much of the “ $u-v$ ” plane (see next section) as possible during the source observation time. This leads to the replicated aperture pupil plane being seen as series of arcs which

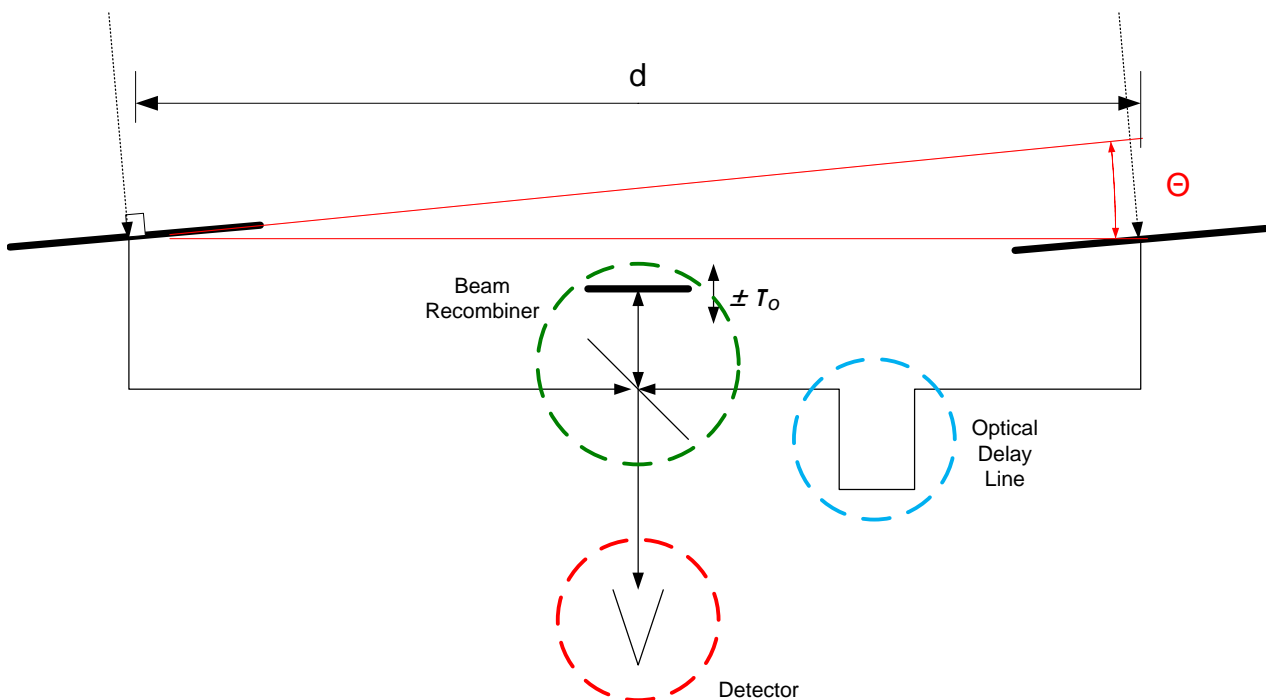


Figure 3: The basic elements of the pupil plane recombination interferometer.

## Far Infra-red Space Interferometer Critical Assessment

naturally means that the amount of spatial frequencies in the reconstructed image is much reduced. Standard and well understood methods, mostly from radio astronomy such as *MaxEnt* or *CLEAN*, can then be used to recover the images at the maximum spatial resolution available in the native data.

### 3.3 The u-v Plane and the Visibility Function

A more convenient, and standard, method to express the spatial coverage of an interferometer is to refer the “u-v” plane. Here where the vectors describing the positions of the interferometer apertures are referred to wavelength normalized positions in the effective aperture plane. In simple terms if  $\mathbf{b}$  is the vector relating the positions of the apertures then we write  $u=b_x/\lambda$ ,  $v=b_y/\lambda$  and  $w=b_z/\lambda$ . In practice the third (axial) term is not used and the aperture coverage is described in terms the “u-v plane”. If the sky co-ordinates of the source are similarly decomposed in terms  $(l,m)$  (i.e. in RA and Dec) we can relate the source distribution to the sampled u-v plane through the visibility, or mutual coherence, function:

$$V(u,v) = e^{-2\pi i w} \iint A(l,m) I(l,m) e^{-2\pi i (ul+vm)} dl dm \quad (2)$$

Here A is the angular response function of the primary beam of an antenna, I is the source distribution and the term  $e^{-2\pi i w}$  describes any phase errors due to displacement of the antennas axially etc (we can ignore this). We can see then that the basic field of view of our interferometer is given by the angular response function of a single antenna within the array. Given all things are equal this will be  $\sim \lambda/D$ . Inversion (i.e. the Fourier transform) of  $V(u,v)$  recovers the source distribution as expected from the van-Cittert-Zernike theorem.

### 3.4 The “Double-Fourier” method

In the “double-Fourier” proposed by Mariotti and Ridgeway (1988) [17], the proposal is to use a more or less continuously scanning system on a space platform. In this way the optical delay line is either dispensed with or added in a symmetrical architecture as the source will always be close to the “zenith” as the entire system is pointed towards the source. The moving mirror in the re-combiner unit now acts as both the optical fringe tracker and as the moving element in a Fourier Transform Spectrometer. As  $d$  changes so does the spatial fringe content and the spectral content is found from the detailed interferogram recorded as the re-combiner mirror is moved. As this is the technique of choice for the interferometer, we have studied it in detail as part of the FISICA programme. We refer to the more detailed section on telescope and instrument requirements (Deliverables 1.2 and 1.3) for a more in-depth analysis of the implications of the interferometer performance.

### 3.5 The “multi-Fourier” method (Mu-FT)

In the “multi-Fourier” proposed by Ohta, Hattori and Matsuo (OHM05) (2005) [14], and implemented in Ohta, Hattori, Matsuo (OHM05) (2007) [18], the proposal is to use a similar system to above employing a Martin-Pupplet type scanning FTS. OHM05 make a change to equation 2 to show how the spatial and spectral content are

## Far Infra-red Space Interferometer Critical Assessment

simultaneously recorded within the mutual coherence function. Dropping the axial phase term for clarity:

$$V(u, v, \nu) = \iint A(l, m, \nu) I(l, m, \nu) e^{-2\pi i(ul+vm)} dl dm \quad (3)$$

We can see that we can, in principle evaluate the source distribution at any explicit frequency  $\nu$  determined from the measured “spectral” fringe over  $\pm \tau_0$  – the effective distance used in the scanning beam recombiner. Here, unlike OHM05, we have retained the explicit dependence of the antenna aperture function  $A(l, m, \nu)$ . This is referred to by OHM05 as they point out that the system will have different spatial resolution dependent on frequency – it is also clear from (3) that the field of view of the system will also be dependent on frequency. In fact OHM05 go on to point out that the field of view of the MuFT interferometer will be limited by the spectral resolution of the system to:

$$\theta < \frac{(c/\Delta\nu)}{d_{max}} \quad (4)$$

So for a resolving power of 2000 at 4.7 THz and a maximum separation of 20 m we get a FoV of  $\sim 20$  arcmin. As the resolving power decreases (i.e. we look for a broader band spectral response) the FoV also decreases: it would reduce to  $\sim 1$  arcmin at  $R=100$  for our test case for instance.

The net effect of all these considerations is that for the MuFT method the response and performance is a complex mix of spectral and spatial resolution, aperture response, source spectrum and source distribution similarly to the double-Fourier explored more in detail and subject to further study as part of the continuing FISICA programme.

### 3.6 The FISICA Study Selection

In this section we have looked at the basic mathematics behind direct detection interferometers and introduced the concept of the visibility fringe, the  $u$ - $v$  plane and touched on the basic tenets behind the double Fourier interferometer. The science and technical evaluation behind FISICA has led to a selection of double Fourier as the preferred technique in the Far infrared. The primary reason for this selection is its broad instantaneous wavelength coverage combined with the fact that it can be readily adapted to existing focal plane technologies for FIR detector arrays such as Transition Edge Sensors (TES [19]) or Kinetic Induction Detectors (KIDS [20]). The use of focal plane arrays means that the technique can in principle be used to fully maximize the FoV in a relatively straight forward manner. A detailed study into how this works in practice is being undertaken and will be reported in other deliverables.

In the final section of this document we discuss an alternative scheme creating a large aperture telescope using direct recombination of sparse arrays of apertures in a Fizeau configuration.

## 4 Focal plane recombination in more detail

---

The majority of the FISICA programme is devoted to a detailed investigation of all aspects of the “double Fourier” implantation of a direct detection interferometer. We have also undertaken a short study into a focal plane recombination Fizeau interferometer using a fixed pattern of dishes; more akin to a “hyper telescope” ([21], [22]). Here we take a deeper look at how such systems work starting from the choice of sparse array distribution, the theory behind any choice and some model results on the imaging performance of such a system. We go on to look at how alignment and manufacturing errors impact on the performance and set some limits on the performance.

We begin with a discussion of the basic principles behind a class of sparse aperture arrays that provide the optimum u-v plane coverage for the minimum number of dishes.

### 4.1 Golay non-redundant arrays

The issue of how to best distribute a large optical collecting area has been revised in the past both qualitatively and quantitatively [21] [22]. A good discussion is provided by Meinel and Meinel [22], where the optical performances of several sparse aperture arrays were analysed. In this paper two requirements were identified as the most stringent in the process of choice of the optimal apertures configuration. The first one is the ability of covering the uv plane enough to avoid loss of desired information at a certain spatial frequency with the fewest segments, whilst the second one is related to the question on how to achieve an acceptable integration time to allow enough signal-to-noise ratio to allow image reconstruction to be performed.

Amongst the configurations suggested, the ones classified under Golay non-redundant arrays were chosen for the analysis of the performances of non-redundant systems. These types of configurations were given in a paper by Golay [23] where he described possible configurations having compact, non-redundant autocorrelation functions.

A primary goal of sparse aperture imaging is to enhance resolution while minimizing the total light collection area. This delivers the same resolution as a filled aperture but with a significant reduction in size and weight.

Golay failed to describe the original algorithm he used to calculate the non-redundant configurations, therefore pipelines suggested in different articles [22], [24], [25]) were used to give a mathematical representation of its arrays. Following the description given in [22] two configurations were selected, Golay-3 (three apertures array) and Golay-6 (six apertures array) which geometry is represented in Figure 4. In Figure 5 we show examples of the computed Point Spread Functions (PSFs) for these arrays.

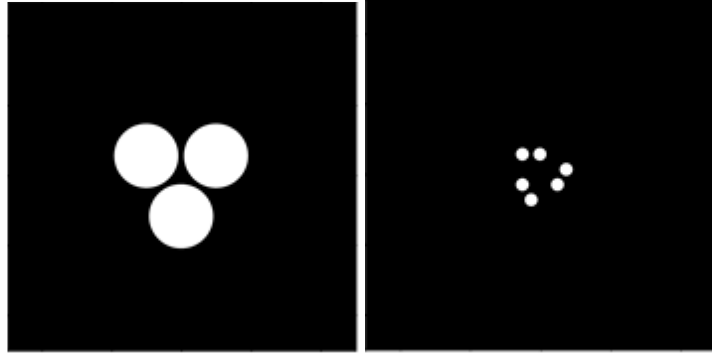


Figure 4: Examples of Golay array distributions. (Left) Golay-3 (right) Golay-6.

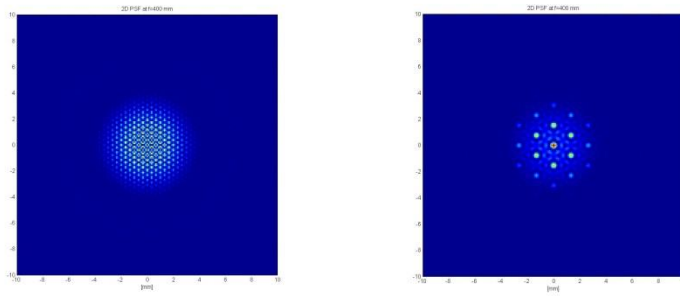


Figure 5: Computed PSF of the simulated Golay arrays shown in figure 5. (left) Golay-3 (right) Golay-6.

#### 4.1.1 Optical theory

Consider a Golay-N sparse aperture array that comprises N identical and circular sub-aperture pupils as shown in Figure 6. In this case one can define  $s$  as the distance between the centers of the two most close apertures and  $d$  the diameter of a single sub-aperture. The ratio  $s/d$  can be defined as the array's expansion factor. It can be noticed that if  $\frac{s}{d} > 2$ , null or holes will appear in the aperture MTF, therefore degrading the image quality, whilst if  $\frac{s}{d} < 1$  the subapertures will overlap. In addition, if  $D_{eff}$  is the minimum diameter of a circular aperture containing all the sparse design considered, the filling factor can be defined as:

$$F = \frac{6d^2}{D_{eff}^2} \quad (5)$$

A sparse array pupil function consisting of N identical subapertures in the  $(x, y)$  plane can be written as:

$$P_{sys}(x, y) = \sum_{n=1}^N P_n(x - x_n, y - y_n) e^{i\varphi_n(x,y)} \quad (6)$$

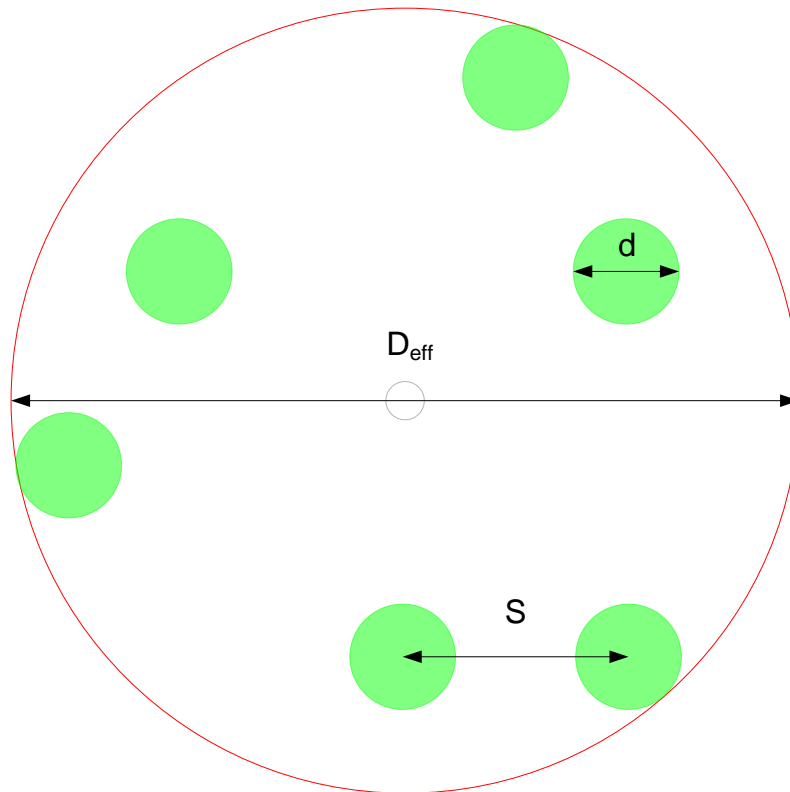


Figure 6: Representation of a Golay 6 aperture showing the parameters used in the text.

where  $P_n$  is the pupil function of a single aperture,  $\phi_n(x, y)$  is the associated phase and  $(x_n, y_n)$  are the coordinates of the  $n^{th}$  sub-aperture in the pupil plane. In order to do a performance analysis of such an imaging system, for an incoherent system two quantities are normally used, the point spread function (PSF) and the modulation transfer function (MTF). The first one is linear in intensity so that the image formed is the convolution of the pupil array PSF and the ideal geometric image intensity, and it can be calculated by taking advantage of the Fourier transform relation obtaining therefore [25], [26], [27]:

$$PSF_{sys}(x', y') = FT\{P_{sys}(x, y)\} \quad (7)$$

where FT indicates the Fourier transform operation and  $(x', y')$  are the image plane coordinates. Ideally, the array PSF would tend to a delta function therefore, a good imaging system would present a narrow central peak containing the majority of the intensity energy. Consequently, this width can be used to characterize the imaging capabilities of the array considered, by doing the ratio between the energy encircled in the central peak and the total one.

In addition, in the spatial frequencies domain, both attenuation and phase information contained in the spatial frequencies of an incoherent image can be expressed through the optical transfer function (OTF) which is the normalized Fourier transform of the PSF. Its modulus, known as MTF (modulation transfer function) describes the transfer of object contrast to an image as a function of spatial frequency. This is a useful metric in evaluating sparse aperture imaging and for N

identical apertures, in phase, it can be demonstrated that OTF and MTF are the same [25] and can be expressed as:

$$MTF = \left| \frac{FT\{PSF_{sys}(x',y')\}}{\iint PSF_{sys}(x',y') dx'dy'} \right| \quad (8)$$

Examples of the MTF's of Golay configurations are shown in Figure 8 corresponding to the PSFs shown in Figure 7.

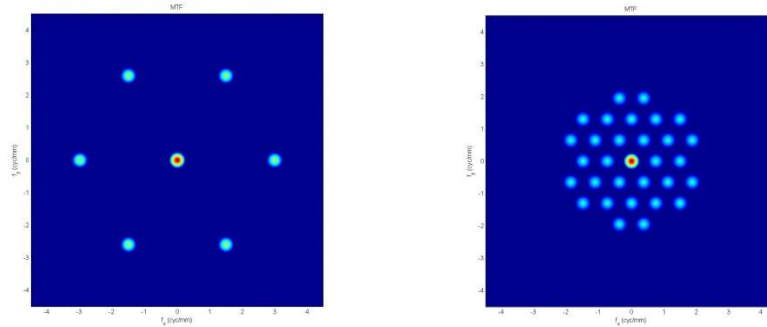


**Figure 7: MTFs of simulated Golay arrays corresponding to PSFs shown in figure 6. (Left) Golay-3 (right) Golay-6.**

The MTF can be used to derive a value for the effective diameter of the overall configuration by analysing how the spatial frequencies are arranged in the considered array of apertures. It can be also used to set a criterion on the limiting detection noise in terms of the MTF frequency attenuation (this is one cause of degradation, although not the only one). These two properties can be used to optimize the performances of a sparse array design by maximizing the MTF maximum spatial frequency cutoff and contrast.

Any aberration within a sub-aperture will necessary reduce the single aperture MTF while phase errors between the sub-apertures will reduce the overall MTF. An ideal MTF has a constant value over an infinite spatial frequency bandwidth, corresponding to an ideal delta function PSF. However, any practical imaging system will have a finite pupil that will limit the overall MTF spatial frequency bandwidth and reduce image contrast at all spatial frequencies relative to the background.

The optimization of the array parameters for a Given Golay arrangement (i.e.  $s$ ,  $d$  and  $D_{eff}$ ) cannot be performed analytically and numerical optimization algorithms are computationally demanding. Nevertheless, for arrays with few sub-apertures it is possible to apply a numerical approach [23], [28]. In this context, arrays with compact, non-redundant arrangements provide a good way to maximize spatial frequency bandwidth with the fewest number of sub-apertures. Some of these configurations were identified as optimal such as the Golay-3, -6, -9, -12 arrays [25].

## 4.2 Feasibility studies and Implementations

Several feasibility studies in the context of sparse aperture imaging for space missions has been made and proved that such Golay array distributions represent a suitable solution for the quest of achieving high angular resolution while containing the satellite costs. Some diffraction limited sparse aperture telescopes have been demonstrated and implemented with active phase control [22]. One of these is the MMTT built by the USA Air Force Research Laboratory [29] which employs a complex laser metrology system to sense wavefront errors and allow the absolute phasing of four 20cm telescopes with 15 arcmin FoV. A more compact design was developed at MIT [30] as pathfinder for a Golay-3 optical satellite (ARGOS), which demonstrated the feasibility of modular space-based optical system with the capability to track fast orbiting objects like the ISS. Due to the tight tolerances of the system, a custom built active control system is used to maintain the system in phase. Finally, a nine aperture system was also developed at Lockheed Martin [31] which has been used for Earth observation purposes and employs a complex active phasing system within each one of the apertures (shown in Figure 8) which allowed a  $1\mu\text{rad}$  phased field of view to be obtained and sampled by 2000x2000 pixel array, requiring 0.05 waves rms on each collector telescope, achieved using wavefront sensing techniques.

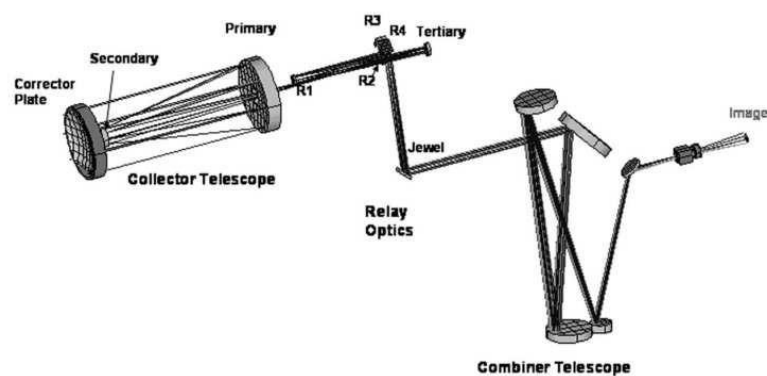


Figure 8: Optical schematic of a single STAR-9 telescope. Image taken from [31].

More recently, a deployable telescope concept for earth observation in a Fizeau configuration has been proposed [32]. The analysis carried out shows the capability of a direct imaging interferometer compared to a Michelson one, showing that the achievable resolution in the first case would be of 25cm from a 500km orbit. Nevertheless, good image quality can be achieved only in the case of a tolerance in the position of the primary mirrors ( $0.4\text{ m}^2$  big) of  $0.1\ \mu\text{m}$ .

In conclusion we note that in all the designs described above, the tightest requirement is in the phasing of the telescope optics. This is achieved through complex wavefront sensing techniques that requires a wider instrument apparatus to be present within the spacecraft, thus limiting the space for science instrumentations and increasing the housekeeping costs of the satellite. One possible way to overcome this, is by taking advantage of the electro optic effect of crystals such as lithium niobate to perform the required phasing without constantly adjusting the position of the main collectors of the telescope. This is currently being studied at UCL OSL (Optical



## Far Infra-red Space Interferometer Critical Assessment

the model was undersampled given the limited computing availability, but a comparison can be made with the properly sampled (but not scaled) G6 one.

### 4.3.1 Piston Error

Piston error, in the formalism described above, is represented by the first term in the Seidel polynomial, which is used to represent a piston movement of  $dh$  at the center of a submirror. For simplicity of representation, it is assumed that only one mirror has a piston deformation.

The two cases analyzed are the ones of a Golay-3 and 6 systems where the following parameters are used:

Wavelength	Subaperture diameter	Effective diameter	Focal length
$10 \mu m$	$100 \mu m$	$533 \mu m$	$900 \mu m$

**Table 1:** list of parameters used in the analysis of piston error.

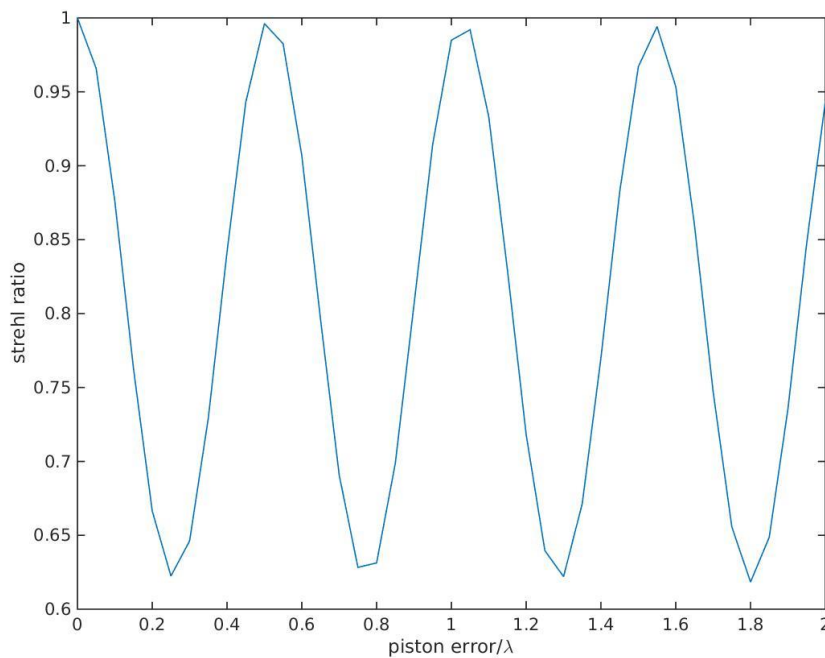


**Figure 10:** Strehl ratio versus piston error for a Golay-3 system.

When analyzing the SR values, a periodicity is seen in both cases as shown in Figure 10 and Figure 11 representing a three and a six aperture system respectively. It comes straightforward to notice that with fewer apertures the SR decreases quickly below 0.8 whilst it remains higher when the number of collecting areas increases to six. Nevertheless, if one looks at the single PSFs it can be seen that features similar to the central peak arise with similar frequency thus diminishing the resolution in similar ways for the two systems. On the contrary, the MTF remains above the limit of  $SR=0.8$  through the interval analysed. It should also be noted that the error produce by the piston could be reduced by combining several baselines (rotation), providing the noise have a white distribution.

In both cases a piston error more than around  $0.1\lambda$  is enough to lower SR below 0.8. We also noted that the periodicity of the oscillation is a factor of 2 higher than the one described in [26].

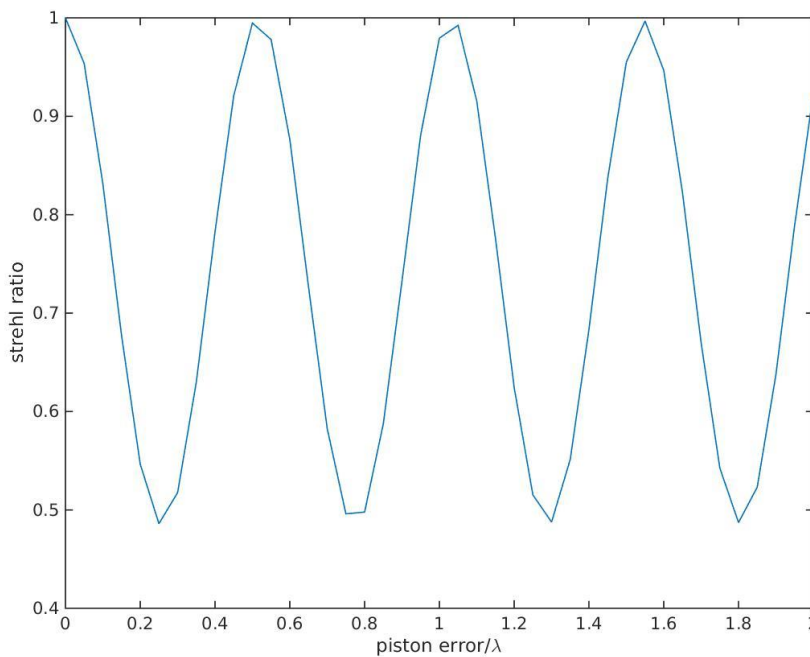


Figure 11: Strehl ratio versus piston error for a Golay-6 system.

Some examples of G3 and G6 with the relative amount of piston error are shown below. G3 in Figure 12 and G6 in Figure 13.

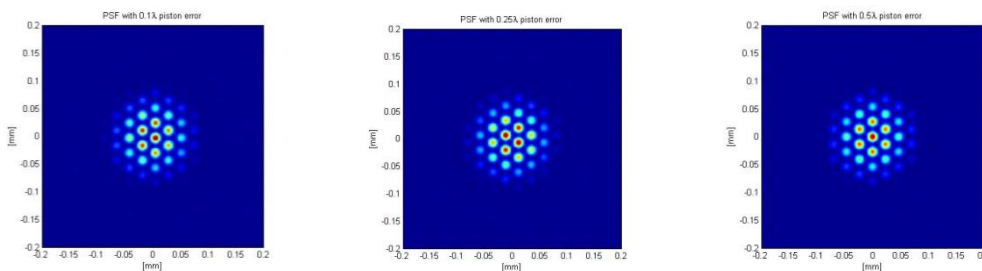


Figure 12: From left to right, Golay-3 system PSF with piston error of 0.1, 0.25, 0.5  $\lambda$ .

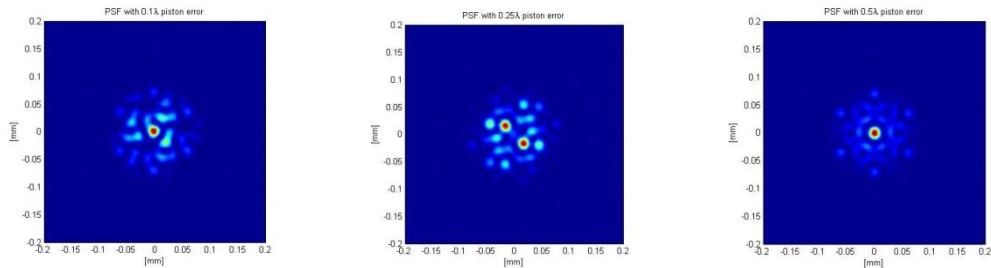


Figure 13: From left to right, Golay-6 system PSF with piston error of 0.1, 0.25, 0.5  $\lambda$ .

### 4.3.2 Tilt Error

Similarly to piston error, tilt error can be described with a term of the Seidel polynomial, particularly the third [26] term. Also here for simplicity, it is assumed that this error is applied only to one aperture and the simulation variables are the same as the one described in Table 1.

In this case, when one aperture is tilted enough, SR decreases dramatically, due to the fact that one aperture is not focusing on the same position of the others. This is more sensible in the case of a Golay-3 system where a tilt of  $\sim 0.5\lambda$  is enough to produce a SR lower than 0.8, whilst in the Golay-6 case this limit shifts to  $\sim 0.8\lambda$ , as shown in Figure 14 and Figure 15. In this case the tilt error is expressed in term of peak-valley tilt of the wavefront caused by the mirror tilt:  $PV_{tilt} = n\lambda$ .

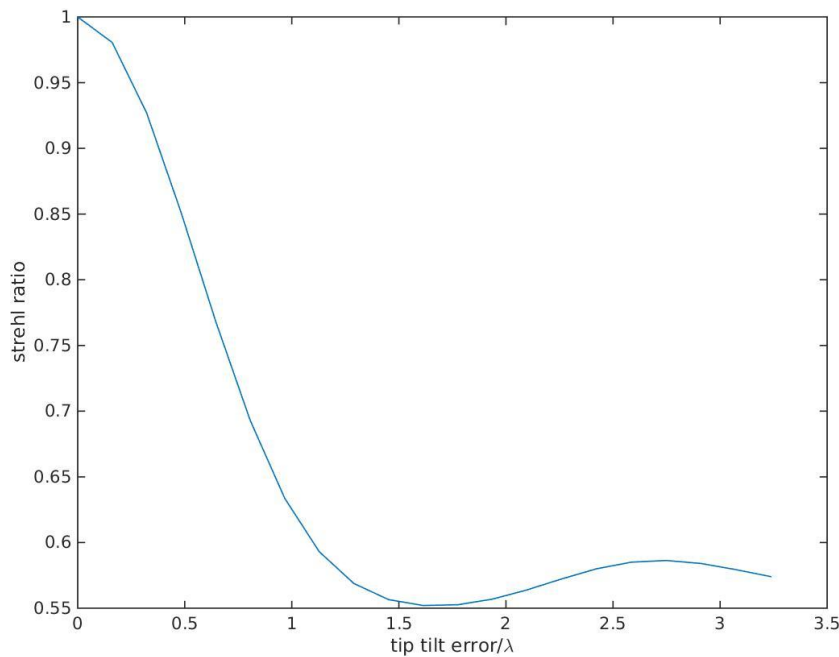


Figure 14: Strehl ratio versus tilt error as a function of  $\lambda$  for a Golay-3 system.

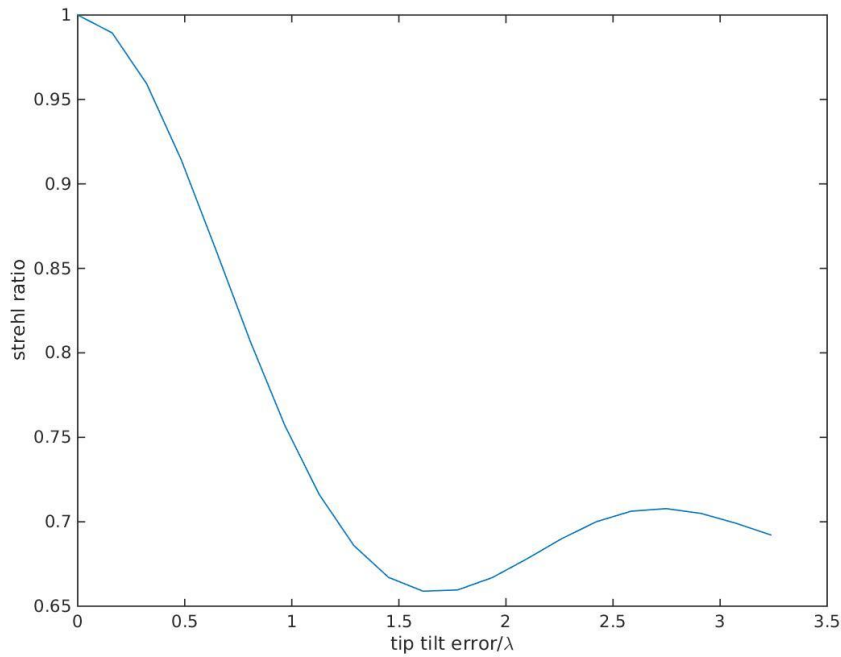


Figure 15: Strehl ratio versus tilt error as a function of  $\lambda$  for a Golay-6 system.

Figure 16 shows the PSF of a Golay-3 system in three tilt cases, it can be seen how one mirror goes out of focus and moves outside the interference pattern, leaving the classical two aperture fringes pattern. Figure 17 instead represents three cases of tilt error in a Golay-6 system, where it can still be seen one aperture moving out of focus.

In this case the effects on MTFs are greater and causes some undersampling of the uv plane losing also the uniform spatial frequency distribution, as can be seen in Figure 18.

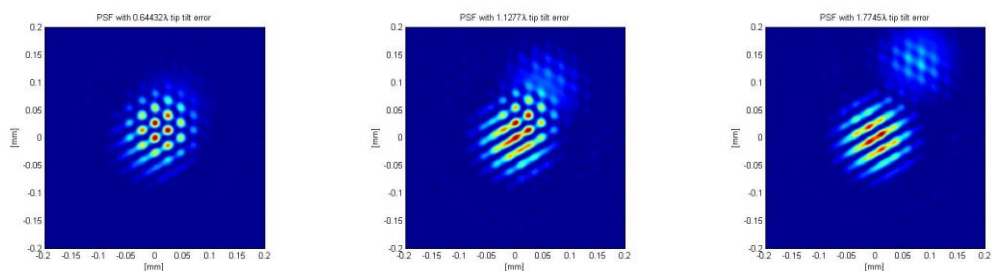


Figure 16: From left to right, Golay-3 system PSF with tilt error of 0.7, 1.3, 1.8  $\lambda$ .

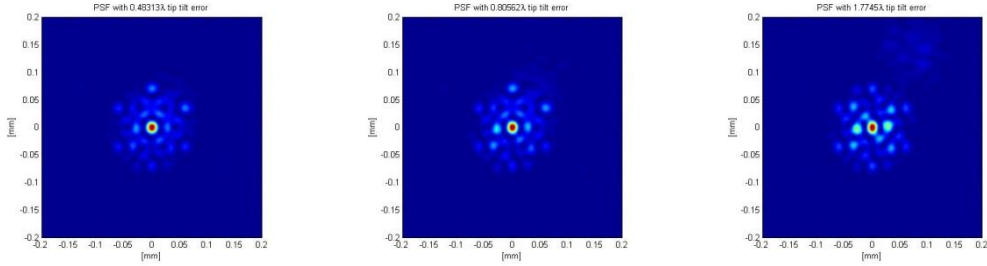


Figure 17: From left to right, Golya-6 system PSF with tilt error of 0.5,0.8,1.8 λ.

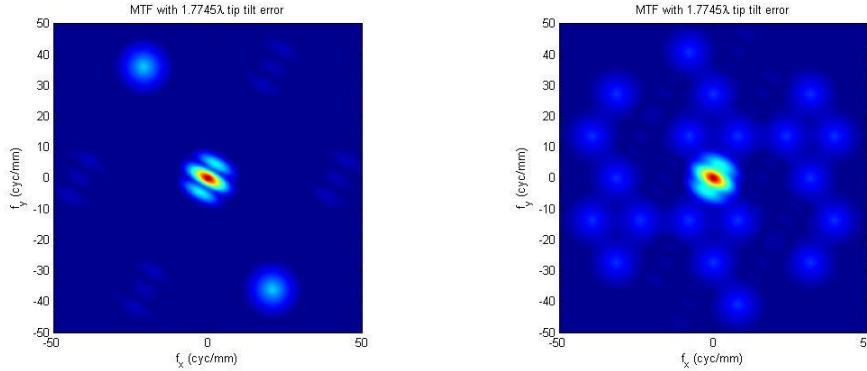


Figure 18: MTF of a Golya-3 (left) and Golya-6 (right) system with tilt error on one aperture of ~1.8λ.

### 4.3.3 Pupil Mapping Error

Coherent imaging with multi-aperture phased array can be seen as composed of two parts. Firstly, pupil mapping occurs between the entrance and exit pupil, then there is a Fourier Transform process that allows to create the coherent image at the focal plane.

To allow coherent imaging over a significant FoV, pupil mapping has to be performed so that the exit pupil form a scaled replica of the entrance one. This is generally called “golden rule” of beam combining.

We followed the approach described in [30] to consider the tolerances on pupil mapping in relation to the FoV that is allowed with such errors. This is done by analyzing how the OPD changes with incorrect system pupil mapping, in particular we consider how the magnification error (between entrance and exit pupil) and shear error causes the FoV to change. For shear error we intend the error caused by the relative difference in the position of the subapertures from perfect alignment.

In general, OPD can be represented as follows:

$$OPD = |B \sin \alpha - b \sin \beta |$$

Where B and b are the baseline distances between two apertures at the entrance and exit pupil respectively, whilst  $\alpha$  is the half FoV value and  $\beta$  is the corresponding magnified one through the system. Having defined a requirement in the phase tolerance of, for example  $\frac{1}{k} \lambda$ , it is possible to set the FoV equation as follows:

$$\frac{FoV}{2} \left| \Delta b m_a + \Delta m_a \left( \frac{B}{m_a} - \Delta b \right) \right| = \frac{\lambda}{k}$$

Where  $m_a = D/d$  is the aperture magnification factor defined as the ratio between the subapertures diameter of entrance (D) and exit (d) pupil.

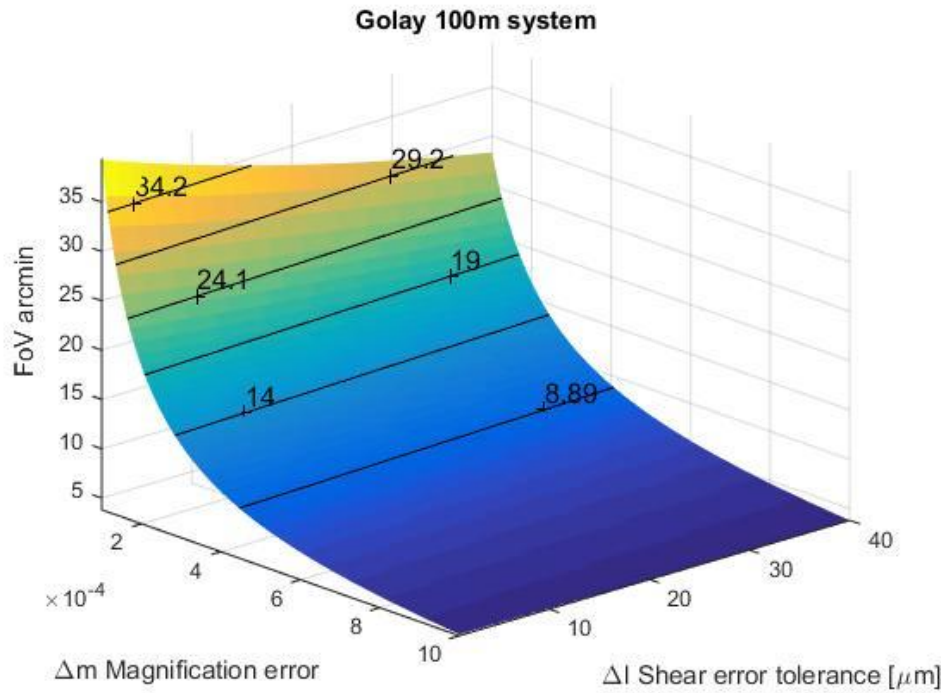


Figure 19: FoV versus pupil mapping tolerances for a Golay system.

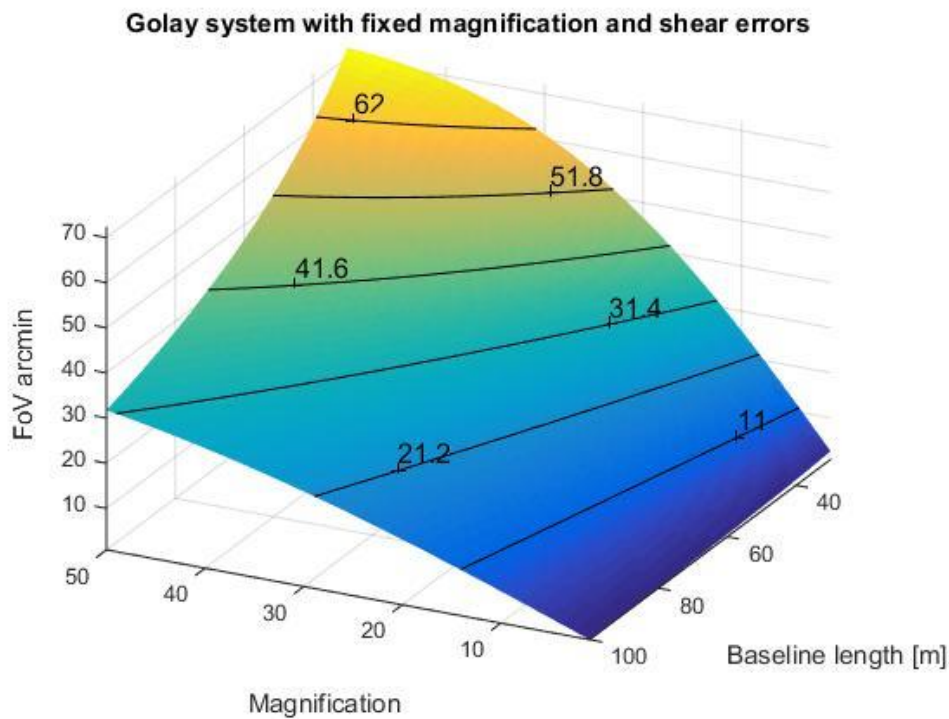


Figure 20: FoV versus magnification and baseline length for a given combination of magnification and shear error.

## Far Infra-red Space Interferometer Critical Assessment

The results are represented in Figure 19 and Figure 20 for a Golay system, these graphs can be used to assess both an array of three and six apertures having assumed the baseline length  $B$  corresponds to the maximum distance between two apertures of the system considered. For the graphs shown above it was considered a system with the characteristics displayed in Table 2.

Wavelength	Entrance pupil subaperture diameter (D)	Exit pupil subaperture diameter (d)	Baseline length (B)	Phase tolerance
$100 \mu m$	$2 m$	$20 cm$	$100 m$	$\frac{\lambda}{10}$

**Table 2: List of variables used in the pupil mapping study.**

Firstly, one can notice from Figure 19 that FoV is sensible both to shear and magnification errors showing a substantial increase in its value when  $\Delta l$  and  $\Delta m$  decreases. Moreover, a minimum value of 5 arcmin is reached in the case of highest error represented, slowly increasing with decreasing  $\Delta m$  until this reaches a value of about  $4 \cdot 10^{-4}$ . In addition, it can also be noticed that shear error contributes less in the value of FoV when  $\Delta l$  is high.

On the contrary, for a fixed value of shear and magnification error, the figures for FoV varies more, as shown in Figure 20. In this case it was chosen a value of  $5 \mu m$  in shear and  $5 \cdot 10^{-4}$  in magnification.

It can be noticed that the highest FoV value is reached for a short baseline and high magnification.

#### 4.3.4 Comparison between a Golay-6 system and FIRI

To complete the assessment of Golay non redundant arrays, a comparison is made between a Golay-6 system with a similar distribution to a FIRI system like the one described in [35]. In particular, for piston and tilt error analysis we choose the primary mirrors to be 2m wide, a baseline length of 100m operating at  $400 \mu m$  with magnification factor of 10 and an equivalent focal length of 200m. These numbers were also chosen to simplify computation capability, but we are required then to consider effects of undersampling in the PSFs calculation that might lead to an imprecise estimation of the actual SR limits.

Figure 21 and Figure 22 show the simulated results. It can be noticed that in the case of piston error, the same periodicity is observed but in this case one aperture shows less effect on SR than the case analyzed in section 4.3.2. In the case of tilt error, a similar behaviour is observed, showing a substantial decrease in SR below 0.8 when the tilt is higher than  $1\lambda$ .

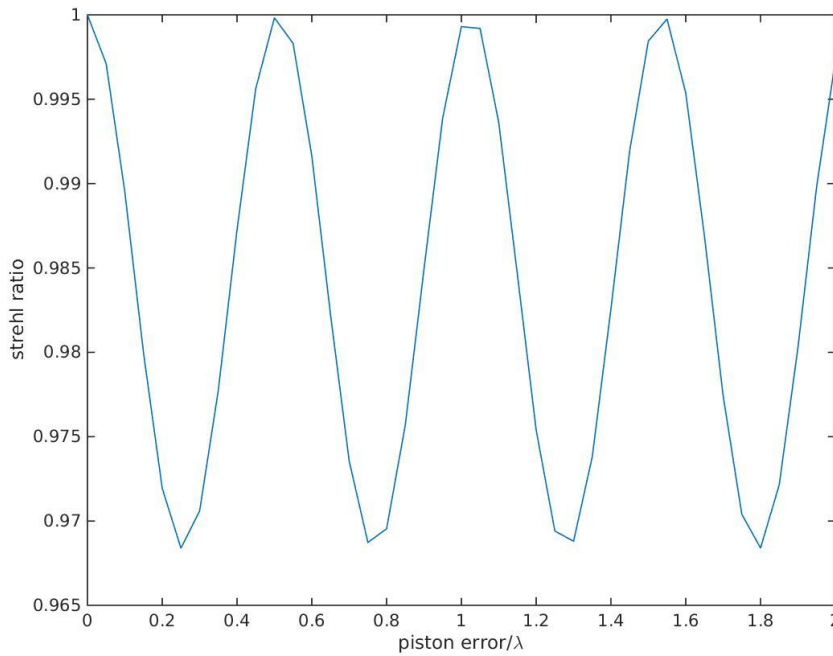


Figure 21: Strehl ratio versus piston error for a Golay-6, FIRI-like system.

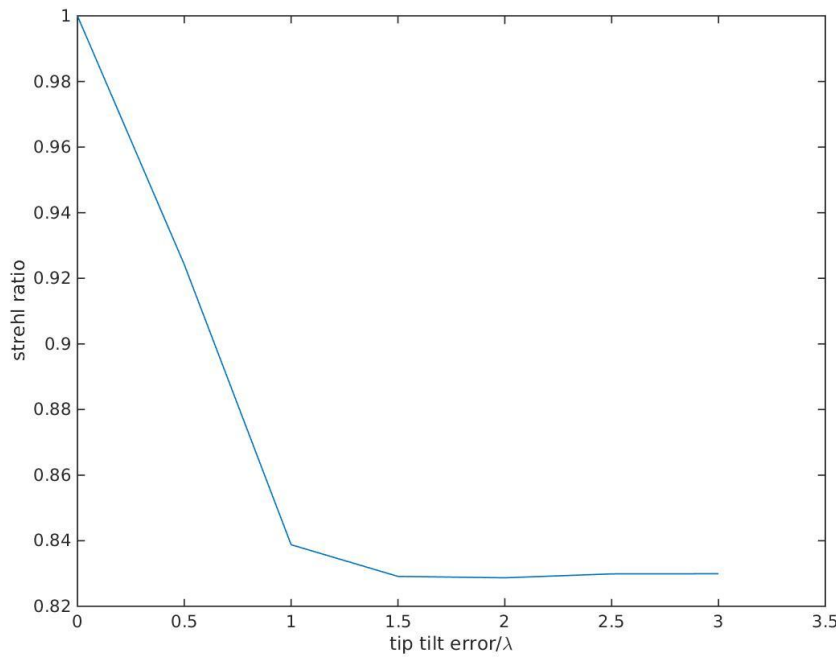


Figure 22: Strehl ratio versus tilt error for a Golay-6, FIRI-like system.

## Far Infra-red Space Interferometer Critical Assessment

More detailed comparisons with a FIRI-like system require detailed knowledge of the magnification of the system which stem from a detailed optical design which is not available at this stage given that many other issues come into play in the FIRI-like system (see deliverable D1.2).

#### 4.4 Pupil densification

Current interferometers involve between 2 and 4 telescopes that can be used simultaneously, therefore the study of faint sources requires many observations and image-reconstruction techniques like aperture synthesis. If considering interferometers with a larger number of apertures, phased with each other, visibility and closure-phase techniques may not be suitable to produce a satisfying signal with a large number of apertures.

Direct imaging involving a single beam combiner might be a simpler alternative to exploit a well-populated optical or infrared array [36], [37]. In this context, a highly diluted array has pupil filling rate that can be described as  $r = n_T \times d^2/D^2$ , where  $n_T$  is the number of telescopes in the array,  $d$  diameter of single element and  $D$  the total diameter of the array. If this value tends to zero, direct imaging can be performed. This condition can be realised thanks to pupil densification techniques [38], [39].

Labeyrie [40], [41], [38], [39], shows that direct imaging at the focus of a diluted array can be done if the pupil is densified. This can be achieved by either zooming each sub-aperture or by placing them closer (thus providing a significant gain in sensitivity) provided that the original array geometry is preserved. Theoretically, pupil remapping does not alter any useful information, however in comparison with the homothetic arrangement, the Labeyrie “hypertelescope” provides direct imaging only on a limited FoV.

The image pattern in a phased hypertelescope with a highly densified pupil can be described as a windowed convolution of the object. In particular it includes a convolution with the object PSF (interference pattern) and a multiplication by a window function. The interference function is created by the undensified part and represents the convolution of a number of Dirac deltas centred at the centres of each sub-aperture, whilst the window function corresponds to the diffraction pattern of a single aperture. At the densified exit the diffractive envelope is shrunk with respect with the central interference peak.

In terms of resolution, with a non-redundant array with  $N$  apertures, Labeyrie claims that the number of resolution elements (resels) that can be directly image is equal to  $N^2$  [39]. Increasing this number will allow to resolve smaller objects but it will decrease the dynamic range of the system. In densified systems, field crowding limitations are identical.

In Fizeau arrays, the interference function is a periodic lattice of peaks with spacing proportional to  $\lambda$ . In white light condition the fields become spectra when moving from the central zero order peak. Among the spectra, the different orientation and dispersion may be considered as a form of encoding for each order. The convolution of

field sources with this interference function adds spectra of different orders in the central windowed zone.

An example of a densified system is shown in Figure 23 and Figure 24. The first set of images show a Golay system with three apertures 10cm wide with a baseline (distance between the apertures) of 1m, which gives an effective diameter of 0.97m. This is simulated for a wavelength of  $100\mu m$  focused at distance of 30 meters.

In this arrangement, it can be seen that the PSF peak is very broad and light is diffused on a wide area at the focal plane.

When the array is densified (Figure 24), it can be seen that the resulting PSF is more compact and the relative intensity higher, compared to the non-densified case. In particular this can be seen by comparing the intensity (shown with an arbitrary scale) of 1D profiles of the respective PSF, where an increase in intensity and compactness can be seen in the densified case, being 2.5 times smaller in baseline.

As expected, this increase in spatial resolution is accompanied with a decrease in the frequencies resolution, as indicated by the decrease in the area covered by the MTF when densified.

A similar behaviour can be observed when comparing a Golay-6 array simulated with the same variables (Figure 25 and Figure 26), having its densified version that differs in the baseline by a factor of two: PSF's intensity peak increases while the spatial frequencies range decreases.

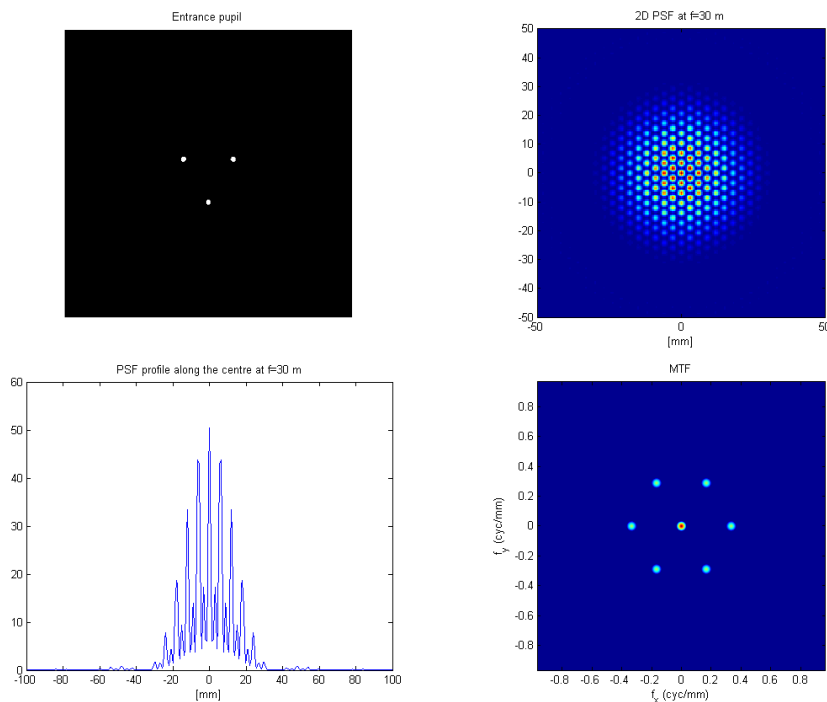


**Figure 23: (top-left) Pupil image of a Golay-3 system. (top-right) Corresponding PSF focused at 30 meters. (bottom-left) PSF profile along the center. (bottom-right) MTF of the simulated Golay-3 system.**

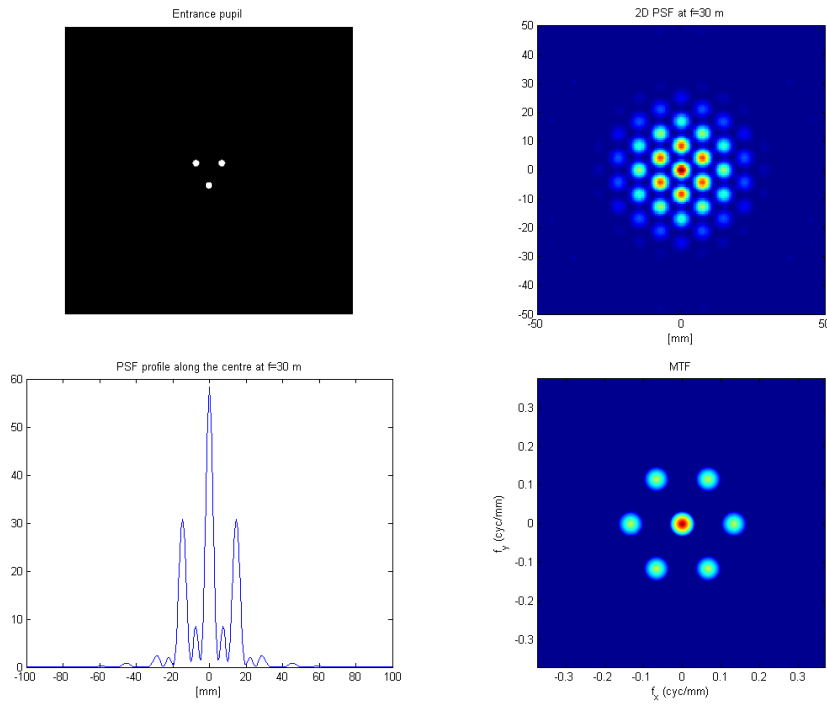


**Figure 24: (top-left) Pupil image of a densified Golay-3 system. (top-right) Corresponding PSF focused at 30 meters. (bottom-left) PSF profile along the center. (bottom-right) MTF of the simulated system.**

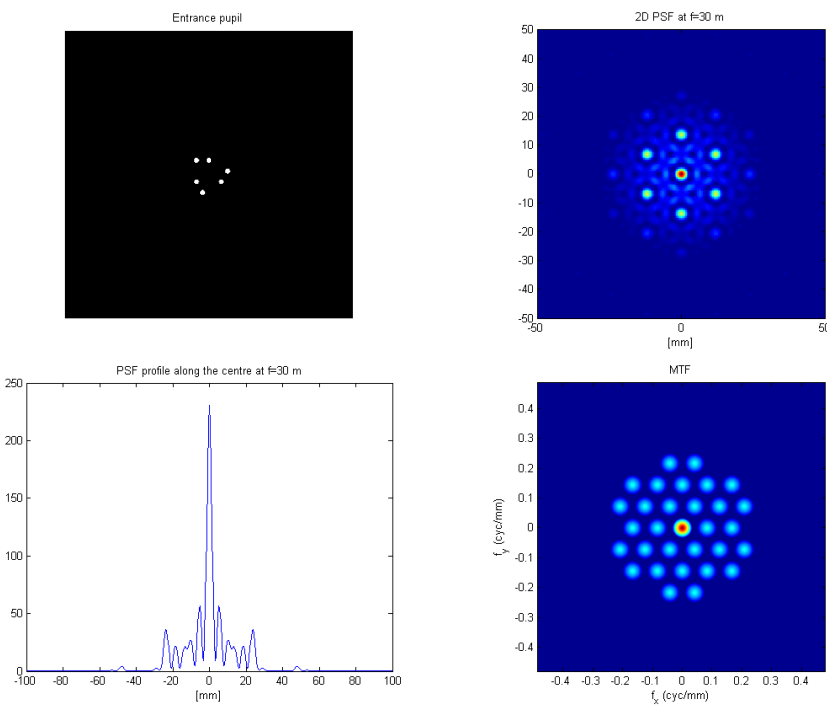


**Figure 25: (top-left) Pupil image of a Golay-6 system. (top-right) Corresponding PSF focused at 30 meters. (bottom-left) PSF profile along the center. (bottom-right) MTF of the simulated Golay-3 system.**

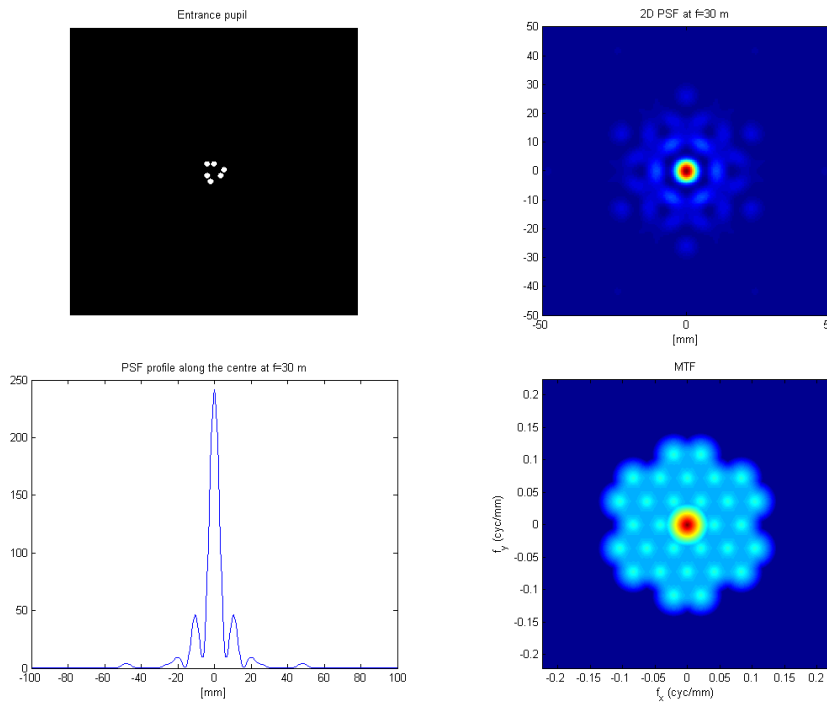


**Figure 26: (top-left) Pupil image of a densified Golay-6 system. (top-right) Corresponding PSF focused at 30 meters. (bottom-left) PSF profile along the center. (bottom-right) MTF of the simulated system.**

#### 4.5 Minimum redundancy linear arrays

There is another class of linear arrays which achieves maximum resolution for a given number of elements by reducing the number of redundant spacings present in the array. This has been studied by Moffet [42] for the design of a radio array to observe faint extragalactic sources, where he based its study on the requirements on integration time and collected power. Being linear arrays they rely on rotation (of the Earth in this case) to fully populate the 2-D u-v plane. In principle a rotating system in space could achieve the same purpose.

Once the element size of an array is defined, it is possible to estimate the optimum array that will give the maximum resolution. These arrays have the following properties:

1. Each spacing is present only once;
2. Each element is spaced by a multiple of unit spacing ( $u_0$ );
3. Each array samples the spatial frequencies spectrum out to a spacing given by  $u_{\max} = 1/2N(N-1)u_0 = N_{\max}u_0$  for possible pairs of N distinct elements;
4. Redundancy can be defined by  $R = \frac{N(N-1)}{N_{\max}}$ . Additionally, the resolution achievable with such arrays can be improved by considering the Earth rotation synthesis.

Figure 27 shows an example of a minimum redundancy linear array of five apertures. The simulation was done at a wavelength of  $100\mu m$  with apertures of 10cm and a distance between the closest apertures of 1.5m, focused 30 meters away.

It can be seen that a good coverage in the spatial frequencies (MTF) is achieved on one dimension and the  $u,v$  plane can ideally be filled (well) by rotating the array. The PSF shows several artifacts that spread around the high intensity central peak. Given the good level of 1 dimensional spatial frequencies covered such an array could perform well as it is rotated providing instantaneous coverage is not an issue.

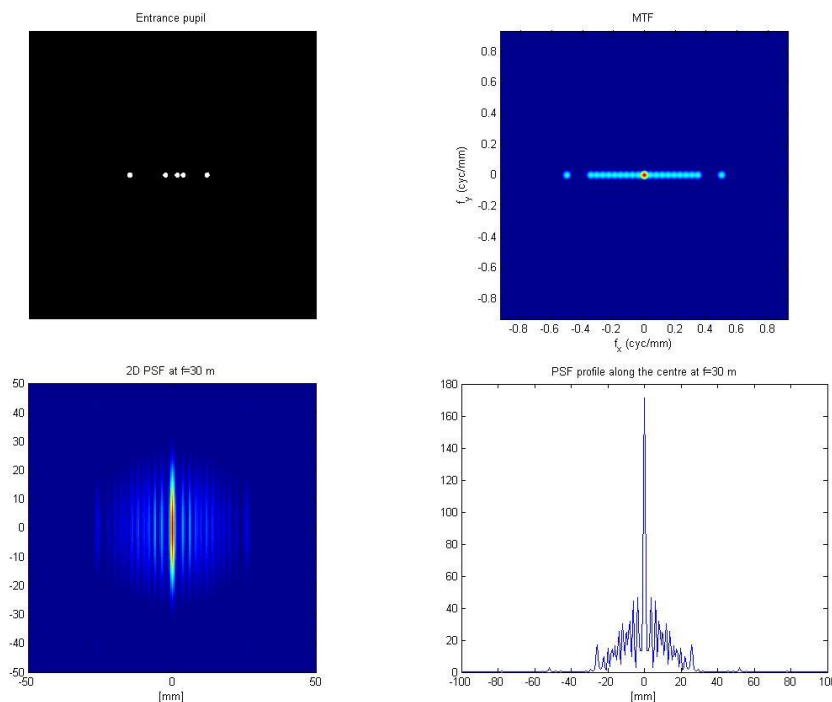


**Figure 27: (top-left) Pupil image of a 5 aperture linear array. (top-right) Corresponding MTF. (bottom-left) 2D PSF. (bottom-right) 1D PSF.**

## 5 Summary – pursuing technical implementation

In this document we have given an overview of the various methods of directly combining the light from sparsely distributed apertures to make images with the spatial resolution of a much larger single telescope. We have tried to expose where the theoretical and practical difficulties lie in achieving such a facility. Two systematic approaches appear the most promising for a future large aperture space mission to observe in the FIR:

1. A double-Fourier interferometer using two dishes and a recombining hub
2. A multiple aperture focal plane recombination telescope in a Fizeau configuration.

Looking at the practicalities of the first option, both pupil plane and two aperture homothetic interferometers have been proposed for the FIR (Leisawitz et al Astrophys.

## Far Infra-red Space Interferometer Critical Assessment

Space Sci. 269(1999), Kohyama et al SPIE 7013 (2008)) and are the subject of study for balloon borne demonstrators with small (40 cm) collecting apertures. There are significant practical issues associated with these systems not the least of which is the necessity of keeping the optical systems aligned with each other to within the coherence length of the light which is characterised by the fractional instantaneous spectral bandwidth of the system ( $R=\lambda/\Delta\lambda$ ) times the wavelength i.e. coherence length  $\sim R\lambda$ . For a typical 10% bandwidth at 50-100  $\mu\text{m}$  this means keeping the system co-axially stable to within 5-10  $\mu\text{m}$  over the typical observational periods – possibly up to several hours. This has proved challenging even for balloon borne instruments with small apertures; for separate spacecraft it is an even greater problem and studies to date have concentrated on “structurally connected” systems employing just two modest ( $\sim 1$  m) apertures (Leisawitz et al Adv. Sp. Res., 40 (2007)). The studies show that such systems should be practical and could be implemented on space platforms. Much detailed work remains however and identifying real technical solutions to the problems need to be identified and development work undertaken. This is the subject of the continuing FISICA programme.

We looked in some detail at the second option including looking at optimal array configurations and the use of “pupil densification” to manipulate the shape of the PSF. Solutions can definitely be found for such systems using Golay non-redundant arrays with phase correcting optics and practical examples have been discussed. However, they are all complex and the methods and tolerance requirements for co-phasing the apertures in a Fizeau system are stringent. Although such a system in principle only requires static co-phasing – i.e. once the apertures are brought into phase once the system will be operational – in practice this is not likely to be true due to thermal distortions typical of space facilities and constant adjustment and re-alignment will be needed. Good imaging has been demonstrated and many systems continue to be developed especially for direct imaging of exoplanets for instance, however the practical difficulties of implementing such a system are clearly not less than those for option 1 and achieving good imaging performance over a reasonable field of view remains challenging.

The FISICA programme is above all about identifying the technical and practical needs of a future FIR high spatial resolution facility. In consideration of this, of the work already undertaken at the start of the programme and the practical and theoretical difficulties exposed in our short study of the Fizeau systems we feel that a deep study into the double-Fourier method is the best course to take for the remainder of the FISICA study period. Work will continue on the Fizeau system but at a lower level and concentrating on providing experimental data to supplement the modelling approach.

## 6 Bibliography

---

- [1] C. van der Avoort, S. F. Pereira, J. J. M. Braat and J.-W. den Herder, "Optimum synthetic-aperture imaging of extended astronomical objects.," *Journal of the Optical Society of America. A, Optics, image science, and vision*, vol. 24, no. 4, pp. 1042-52, #apr# 2007.
- [2] A. Labeyrie, S. G. Lipson, P. Nisenson, . Labeyrie, . Lipson and . Nisenson, "An Introduction to Optical Stellar Interferometry," *An Introduction to Optical Stellar Interferometry*, 2006.
- [3] R. H. Brown and R. Q. Twiss, "Interferometry of the Intensity Fluctuations in Light II. An Experimental Test of the Theory for Partially Coherent Light," *Proceedings of the Royal Society A: Mathematical, Physical and Engineering Sciences*, vol. 243, pp. 291-319, 1958.
- [4] J. Zmuidzinas, "Thermal noise and correlations in photon detection.," *Applied optics*, vol. 42, no. 25, pp. 4989-5008, 2003.
- [5] G. Kirkbright, *R. Hanbury Brown: the intensity interferometer-its application to astronomy*, vol. 30, 1975, p. 487.
- [6] A. Ofir and E. N. Ribak, "Offline, multidetector intensity interferometers - I. Theory," *Monthly Notices of the Royal Astronomical Society*, vol. 368, pp. 1646-1651, 2006.
- [7] D. Dravins and T. Lagadec, "Stellar intensity interferometry over kilometer baselines: Laboratory simulation of observations with the Cherenkov Telescope Array," no. June, p. 18, #jul# 2014.
- [8] FISICA consortium, "FISICA Deliverable D1.1: Definition/update of key science questions and relevant dat products," 2014.
- [9] ALMA Observatory, [Online]. Available: <http://www.almaobservatory.org/en/press-room/press-releases/771-revolutionary-alma-image-reveals-planetary-genesis>. [Accessed 19 Jan 2015].
- [10] M. A. Johnson and C. H. Townes, "Quantum effects and optimization of heterodyne detection," *Optics Communications*, vol. 179, pp. 183-187, 2000.
- [11] P. Amplifiers, *Parameteric Amplifiers*.
- [12] W. Wild, T. de Graauw, F. Helmich, A. Baryshev, J. Cernicharo, J. R. Gao, A. Gunst, A. Bos, J.-W. den Herder, B. Jackson, V. Koshelets, H.-J. Langevelde, P. Maat, J. Martin-Pintado, J. Noordam, P. Roelfsema, L. Venema, P. Wesselius and P. Yagoubov, "ESPRIT: a study concept for a far-infrared interferometer in space," in *Proceedings of SPIE*, 2008.
- [13] B. Swinyard and T. Nakagawa, "The space infrared telescope for cosmology and astrophysics: SPICA A joint mission between JAXA and ESA," *Experimental Astronomy*, vol. 23, no. 1, pp. 193-219, 2008.
- [14] I. Ohta, M. Hattori and H. Matsuo, "Development of a multi-Fourier-transform interferometer: fundamentals," *Applied Optics*, vol. 45, pp. 2576-2585, 2006.
- [15] M. Born and E. Wolf, *Principles of Optics*, 7th ed., Cambridge univ. pr., 2001.
- [16] W. a. Traub, "Combining beams from separated telescopes.," *Applied optics*, vol.

## Far Infra-red Space Interferometer Critical Assessment

- 25, no. 4, p. 528, 1986.
- [17] S. J.-M. Mariotti, "Double Fourier spatio-spectral interferometry: combining high spectral and high spatial resolution in the near infrared," *Astronomy & Astrophysics*, vol. 195, pp. 350-363, 1988.
- [18] I. Ohta, M. Hattori and H. Matsuo, "Development of a multi-Fourier-transform interferometer: imaging experiments in millimeter and submillimeter wave bands," *Applied Optics*, vol. 46, pp. 2881-2892, 2007.
- [19] K. D. Irwin and G. C. Hilton, "Transition-Edge Sensors," *Applied Physics*, vol. 99, pp. 63-150, 2005.
- [20] P. K. Day, H. G. LeDuc, B. A. Mazin, A. Vayonakis and . Zmuidzinas, "A broadband superconducting detector suitable for use in large arrays," *Nature*, vol. 425, pp. 817-821, 2003.
- [21] F. Boone, "Interferometric array design: Optimizing the locations of the antenna pads," *Astronomy and Astrophysics*, vol. 377, no. 1, pp. 368-376, #oct# 2001.
- [22] A. B. Meinel and M. P. Meinel, "Large sparse-aperture space optical systems," *Optical Engineering*, vol. 41, no. 8, p. 1983, #aug# 2002.
- [23] M. J. E. Golay, "Point Arrays Having Compact , Nonredundant Autocorrelations," *Journal of the Optical Society of America*, vol. 61, pp. 272-273, 1970.
- [24] R. D. Fiete, T. A. Tantaló, J. R. Calus and J. A. Mooney, "Image quality of sparse-aperture designs for remote sensing," *Optical Engineering*, vol. 41, no. 8, p. 1957, #aug# 2002.
- [25] N. J. Miller, M. P. Dierking and B. D. Duncan, "Optical sparse aperture imaging.," *Applied optics*, vol. 46, no. 23, pp. 5933-43, #aug# 2007.
- [26] Q. Wu, J. Fan, F. Wu, J. Zhao and L. Qian, "Error analysis of the Golay3 optical imaging system.," *Applied optics*, vol. 52, no. 13, pp. 2966-73, #may# 2013.
- [27] V. David, *Computational Fourier Optics: A MATLAB Tutorial*, SPIE, 2010.
- [28] E. Keto, "The shapes of cross-correlation interferometers," *The Astrophysical Journal*, vol. 475, pp. 843-852, 1997.
- [29] D. C. Duneman, "Wide field performance of a phased array telescope," *Optical Engineering*, vol. 34, no. 3, p. 876, #mar# 1995.
- [30] S.-J. Chung, D. W. Miller and O. L. de Weck, "Design and Implementation of Sparse Aperture Imaging Systems," *Optical Engineering*, vol. 4849, pp. 181-192, #dec# 2002.
- [31] R. L. Kendrick, J.-n. Aubrun, R. Bell, R. Benson, L. Benson, D. Brace, J. Breakwell, L. Burriesci, E. Byler, J. Camp, G. Cross, P. Cuneo, P. Dean, R. Digumerthi, A. Duncan, J. Farley, A. Green, H. H. Hamilton, B. Herman, K. Lauraitis, E. de Leon, K. Lorell, R. Martin, K. Matosian, T. Muench, M. Ni, A. Palmer, D. Roseman, S. Russell, P. Schweiger, R. Sigler, J. Smith, R. Stone, D. Stubbs, G. Swietek, J. Thatcher, C. Tischhauser, H. Wong, V. Zarifis, K. Gleichman and R. Paxman, "Wide-field Fizeau imaging telescope: experimental results," *Applied Optics*, vol. 45, no. 18, p. 4235, 2006.
- [32] D. Dolkens and J. M. Kuiper, "A deployable telescope for sub-meter resolution from microsatellite platforms," in *ICSO 2014*, 2014.

## Far Infra-red Space Interferometer Critical Assessment

- [33] J. E. Harvey, P. R. Silverglate and A. B. Wissinger, "Optical performance of synthetic aperture telescope configurations," in *SPIE 540, Southwest conference on Optics*, 1985.
- [34] FISICA consortium, "Far Infrared Space Interferometer Critical Assessment," UCL, [Online]. Available: <http://www.fp7-fisica.eu/>. [Accessed 25 02 2015].
- [35] W. Holland and G. Savini, "Instrument requirements from the FISICA study," in *FISICA workshop 2015, Instrument Simulation and Preliminary Technology Development Activities.*, NUIM - Maynooth, 2015.
- [36] O. Lardiere, F. Martinache and F. Patru, "Direct imaging with highly diluted apertures - I. Field-of-view limitations," *Monthly Notices of the Royal Astronomical Society*, vol. 375, no. 3, pp. 977-988, #mar# 2007.
- [37] F. Patru, N. Tarmoul, D. Mourard and O. Lardiere, "Direct imaging with highly diluted apertures - II. Properties of the point spread function of a hypertelescope," *Monthly Notices of the Royal Astronomical Society*, vol. 395, no. 4, pp. 2363-2372, #jun# 2009.
- [38] A. Labeyrie, "Resolved imaging of extra-solar planets with future 10<sup>2</sup>-100 km optical interferometric arrays," *Astronomy and Astrophysics*, vol. 118, pp. 517-524, 1996.
- [39] A. Labeyrie, "Hypertelescope imaging: from exo-planets to neutron stars," in *Proceedings of SPIE*, 2003.
- [40] A. Labeyrie, "Exo-Earth Imager for Exoplanet Snapshots with Resolved Detail," in *ASP Conference Series, vol 194*, 1999.
- [41] A. Labeyrie, L. Arnold, P. Riaud, O. Lardiere, V. Borkowski, S. Gillet, J. Dejonghe and H. Le Coroller, "Hypertelescope architectures for direct imaging at high angular resolution," in *Beyond conventional adaptive optics*, 2001.
- [42] A. T. Moffet, "Minimum-redundancy linear arrays," *IEEE Transactions on Antennas and Propagation*, vol. 16, no. 2, pp. 172-175, #mar# 1968.
- [43] O. Lardiere, A. Labeyrie, D. Mourard, P. Riaud, L. Arnold, J. Dejonghe and S. Gillet, "VIDA ( Vlti Imaging with a Densified Array ), a densified pupil combiner proposed for snapshot imaging with the VLTI .," in *SPIE Interferometry for Optical Astronomy II*, 2003.
- [44] A. Labeyrie, "ELTs, interferometers and hypertelescopes at different wavelengths," vol. 6986, pp. 69860C--69860C--12, #apr# 2008.
- [45] F. Drake, "Optimum size of radio astronomy antennas," *Proceedings of the IEEE*, vol. 52, no. 1, pp. 108-109, 1964.
- [46] M. A. A. and P. F. G., "Measurement of the diameter of  $\alpha$ -Orionis with the interferometer," *Astrophysica Journal*, vol. 53, pp. 249-259, 1921.